JCTC Journal of Chemical Theory and Computation

Article

pubs.acs.org/JCTC

Controlling the Long-Range Corrections in Atomistic Monte Carlo Simulations of Two-Phase Systems

Florent Goujon,[†] Aziz Ghoufi,[‡] Patrice Malfreyt,[*,†] and Dominic J. Tildesley[§]

[†]Institut de Chimie de Clermont-Ferrand, Université Clermont Auvergne, Université Blaise Pascal, BP 10448, F-63000 Clermont-Ferrand, France

[‡]Institut de Physique de Rennes, Université Rennes 1, 35042 Rennes, France

[§]EPFL-CECAM, Batochime (BCH), CH-1015, Lausanne, Switzerland

ABSTRACT: The long-range correction to the surface tension can amount to up to 55% of the calculated value of the surface tension for cutoffs in the range of 2.1−6.4 σ. The calculation of the long-range corrections to the surface tension and to the configurational energy in two-phase systems remains an active area of research. In this work, we compare the long-range corrections methods proposed by Guo and Lu (*J. Chem. Phys.* **1997**, *106*, 3688−3695) and Janeček (*J. Phys. Chem. B* **2006**, *110*, 6264−6269) for the calculation of the surface tension and of the coexisting densities in Monte Carlo simulations of the truncated Lennard-Jones potential and the truncated and shifted Lennard-Jones potential models. These methods require an estimate of the long-range correction at each step in the Monte Carlo simulation. We apply the full version of the Guo and Lu method, which involves the calculation of a double integral that contains a series of density differences, and we compare these results with the simplified version of the method which is routinely used in two-phase simulations. We conclude that the cutoff dependencies of the surface tension and coexisting densities are identical for the full versions of Guo and Lu and Janeček methods. We show that it is possible to avoid applying the long-range correction at every step by using the truncated Lennard-Jones potential with a cutoff $r_c \geq 5\ \sigma$. The long-range correction can then be applied at the end of the simulation. The limiting factor in the accurate calculation of this final correction is an accurate estimate of the coexisting densities. Link-cell simulations performed using a cutoff $r_c = 5.5\ \sigma$ require twice as much computing time as those with a more typical cutoff of $r_c = 3.0\ \sigma$. The application of the Janeček correction increases the running time of the simulation by less than 10%, and it can be profitably applied with the shorter cutoff.

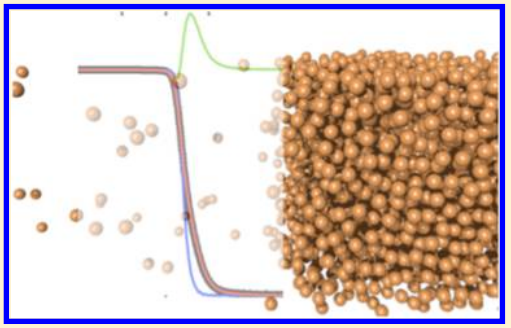

1. INTRODUCTION

Although the first molecular simulations[1−5] of the liquid−vapor interfaces of Lennard-Jones (LJ) fluid using a slab geometry are over 40 years old, important methodological problems associated with these calculations considered the dependence of the interfacial properties on system sizes,[6−10] the range of the interatomic interactions,[9,11−13] the truncation of the potential truncation,[11,14] the mechanical and thermodynamic definitions used for the calculation of the surface tension calculation[14,15] and the long-range corrections to be applied to the surface tension,[14,16−23] and the configurational energy.[19,22−25] As a result of these issues, the comparison between the surface tensions and coexisting densities from different simulations and experiments remains difficult and requires care.

Since most molecular simulations use a pair potential with a spherical cutoff at a distance, r_c, long-range corrections must be added to the thermodynamic properties such as the energy, pressure, stress tensor, and chemical potential to compensate for the missing long-range part of the potential. In the case of bulk simulations,[26] these long-range corrections assume a uniform density, ρ, and a radial distribution function equal to unity beyond r_c. For example, the contribution to the tail corrections to the total energy in the bulk LJ fluid decreases from 12% to 0.4% as the cutoff increases from $r_c = 2.1\ \sigma$ to $r_c = 6.4\ \sigma$. The usual expressions of the long-range corrections to the energy and pressure of a homogeneous system cannot be applied to two-phase systems, and different methodologies have been developed to account for the nonuniformity of the particle density in the slab geometry.

The development of specific long-range corrections for the two-phase simulations and the interfacial properties is an area of active research.[5,12,16−19,22,24,25,27] Unlike the long-range corrections for the energy, the contribution of the tail corrections to the surface tension changes from 50% to 7% as the cutoff changes from $r_c = 2.1\ \sigma$ to $r_c = 6.4\ \sigma$ as shown for the LJ fluid in Figure 1. This significant contribution of the tail correction to the surface tension[11,25] becomes a key factor in quantitatively predicting the surface tension for fluids and fluid mixtures.

Received: April 22, 2015
Published: September 3, 2015

DOI: 10.1021/acs.jctc.5b00377
J. Chem. Theory Comput. 2015, 11, 4573−4585

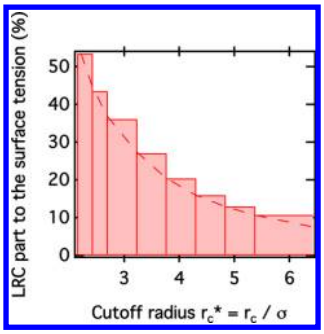

Figure 1. Contribution (%) of the long-range corrections to the surface tension with respect to the total surface tension as a function of the cutoff radius expressed in reduced units. The long-range corrections are calculated with the Janeček methodology using eq 32.

The first expression for correcting the surface tension, developed from the work of Fowler[28] and was originally used by Freeman and McDonald,[29] then subsequently by Chapela et al.[5] and Salomons and Mareschal.[16,17] These expressions are based on a step function for the density profile $\rho(z)$ and hence an interface of zero thickness.

A second approach based on the Kirkwood−Buff expression[30] for the surface tension, proposed initially by Chapela et al.[5] and corrected later by Blokhuis et al.,[18] assumes that $\rho(z)$ can be represented by a hyperbolic tangent function. The resulting expression has been widely used with the truncated Lennard-Jones potential for the calculation of the surface tension of water,[25,31,32] hexane and chlorine,[33] and alkanes.[34] This tail correction is added to the intrinsic (or directly calculated) part of the surface tension at the end of the simulation, and it depends on the shape of the density profile and the density of each coexisting phase. Since these two properties are calculated for the truncated potential without a tail correction, this approach provides a lower bound to the true correction.

A third method is based on the introduction of a local configurational energy[19,22,24,25,35−39] or a local force[36,37] with corresponding local long-range correction, directly into the simulation. This approach was first proposed by Guo and Lu[19,24,35] (GL12) and has been used to correct the energy, pressure, surface tension, and chemical potentials in a slab geometry. A tail correction to the configurational energy, which depends on the position of the molecule in the direction normal to the interface, is included directly in a Monte Carlo simulation and is used in accepting or rejecting a trial move. The long-range correction to the configurational energy is composed of two contributions: the first one is similar to that used for a homogeneous fluid with the local density $\rho(z)$ of the slab replacing the uniform density ρ of the simulation box. The second term corrects the inhomogeneity of the density profile. To date, this second contribution to the correction has been neglected due to the higher computational overhead in its implementation. The simplified method of Guo and Lu (GL1) with the inclusion of only the first term during the course of the simulation has been widely applied for the calculation of the surface tension of various systems.[34,40,41] Another technique based on a similar local long-range correction to the energy was proposed by Janeček.[22] The original version of this technique[22] (JAN) has been extended by MacDowell and Blas[38] to avoid a discretization of the energy into slabs along the direction perpendicular to the interface. The method of Janeček has also been widely applied to different liquid−vapor systems: LJ fluids,[23,38,39] cyclic hydrocarbons,[42] alkanes,[43] water and CO_2[25] and argon.[44] This class of corrections produces a density profile that is consistent with the truncated potential plus its long-range correction.

It is timely to compare the methods of slab-based tail corrections developed by Guo and Lu and Janeček under exactly the same operational conditions. The Monte Carlo simulations, performed using a parallel algorithm, have allowed us to make a detailed comparison with the simulations in the literature and with experiment (with reference to liquid methane). In this work, we have chosen to calculate the surface tension using the mechanical route through the Kirkwood−Buff[30] and Irving and Kirkwood (IK)[30,45,46] definitions because we have established in several previous studies[14] that the different approaches[15] lead to the same surface tension[9,14] once the appropriate long-range corrections are added.

A fourth approach, which represents an alternative to the methods of slab-based tail corrections, consists of modeling the full LJ potential by calculating the long-range dispersion term of the LJ potential using a lattice sum. Initially, the Ewald sum was used to treat the long-range dispersion interactions.[12,27,47,48] This is an expensive approach in which an atom in the central box interacts with all its periodic images. This issue can be overcome by more efficient evaluations of these sums: the particle−particle−particle−mesh (PPPM) Ewald solvers[49,50] and the multilevel summation or tree methods.[51] A recent study[49] has established that the simulations of the liquid−vapor interface of the LJ fluid with the Ewald and PPPM methods for the calculation of the dispersion interactions shows no dependence of the surface tension on the cutoff using PPPM and a slight dependence using the Ewald method. We will use the surface tensions of the LJ fluid calculated in the study[49] of Isele-Holder et al. to compare with our results.

In this work, we focus on the two most used slab-based tail methods and we want to answer to the following questions. Do the methods GL1, GL12, and JAN give the same results for the long-range corrections applied to the same set of liquid configuration in the slab geometry? Which is the most efficient of these methods to use? Is the simplified version of the method of Guo and Lu (GL1) accurate enough to be used? Is it absolutely necessary to include the long-range corrections at every step? If not, what value of the cutoff should we employ for the truncated potential?

The remainder of the work is organized as follows. Section 2 describes the different potential models that we employ in this study: the truncated, the truncated and shifted, and the truncated plus local long-range corrections. Section 3 describes the calculation of the surface tension and section 4 the details of the Monte Carlo simulations. In section 5 we discuss the relative accuracy of the approaches and we provide a detailed analysis of the cutoff dependence of the surface tension and coexisting densities for the different models presented. Section 6 contains our conclusions.

2. POTENTIAL MODEL

Although this is primarily a methodological study, involving the Lennard-Jones fluid, we will occasionally compare the simulated results with those of liquid methane. Actually, the CH_4−CH_4 interaction can be modeled as a single dispersion interaction, ignoring the permanent electrostatic interactions. The intermolecular potential is[52]

DOI: 10.1021/acs.jctc.5b00377
J. Chem. Theory Comput. 2015, 11, 4573−4585

$$u_{\mathrm{LJ}}(r_{ij}) = 4\epsilon_{ij}\left[\left(\frac{\sigma_{ij}}{r_{ij}}\right)^{12} - \left(\frac{\sigma_{ij}}{r_{ij}}\right)^{6}\right] \tag{1}$$

where r_{ij} is the distance between atoms i and j. The LJ parameters are σ_{ij} = 3.7327 Å and ϵ_{ij}/k_B = 149.92 K, where k_B is Boltzmann's constant. The simulations are performed using three variations of this potential. The first, most commonly used in simulation, involves truncating spherically the potential at the cutoff radius (r_c) and is referred to as U_{ST} in this work. Considering a system of N atoms, the total configurational energy U_{ST} is

$$U_{\mathrm{ST}} = \sum_{i=1}^{N-1}\sum_{j=i+1}^{N} u_{\mathrm{ST}}(r_{ij}) \tag{2}$$

where the pair separation distance r_{ij} is calculated by using the minimum image convention and $u_{\mathrm{ST}}(r_{ij})$ is defined by

$$u_{\mathrm{ST}}(r_{ij}) = \begin{cases} u_{\mathrm{LJ}}(r_{ij}) & r_{ij} < r_c \\ 0 & r_{ij} \geq r_c \end{cases} \tag{3}$$

The second variation is the spherically truncated and shifted model (STS) where

$$U_{\mathrm{STS}} = \sum_{i=1}^{N-1}\sum_{j=i+1}^{N} u_{\mathrm{STS}}(r_{ij}) \tag{4}$$

$$u_{\mathrm{STS}}(r_{ij}) = \begin{cases} u_{\mathrm{LJ}}(r_{ij}) - u_{\mathrm{LJ}}(r_c) & r_{ij} < r_c \\ 0 & r_{ij} \geq r_c \end{cases} \tag{5}$$

In the third version, we add a long-range or tail correction to the truncated potential. In a two-phase simulation of a planar interface, the density is a strongly varying function of z. The simulation box is divided into N_s slabs of width δz. Each slab, which is parallel to the interface, has a volume $V_s = L_x L_y \delta z$, and z_k defines the center of the kth slab.

In the simpler version of the Guo and Lu correction, GL1,

$$U_{\mathrm{ST}}^{\mathrm{GL1}} = \sum_{i=1}^{N-1}\sum_{j=i+1}^{N} u_{\mathrm{ST}}(r_{ij}) + U_{\mathrm{LRC}}^{\mathrm{GL1}} \tag{6}$$

where

$$U_{\mathrm{LRC}}^{\mathrm{GL1}} = \sum_{k=1}^{N_s} u_{\mathrm{lrc}}^{(1),\mathrm{GL}}(z_k) \tag{7}$$

and the local term $u_{\mathrm{lrc}}^{(1),\mathrm{GL}}(z_k)$ is given by eq 10.

In the full version, GL12,

$$U_{\mathrm{ST}}^{\mathrm{GL12}} = \sum_{i=1}^{N-1}\sum_{j=i+1}^{N} u_{\mathrm{ST}}(r_{ij}) + U_{\mathrm{LRC}}^{\mathrm{GL12}} \tag{8}$$

where

$$U_{\mathrm{LRC}}^{\mathrm{GL12}} = \sum_{k=1}^{N_s} (u_{\mathrm{lrc}}^{(1),\mathrm{GL}}(z_k) + u_{\mathrm{lrc}}^{(2),\mathrm{GL}}(z_k)) \tag{9}$$

The second term of the local long-range corrections to the energy $u_{\mathrm{lrc}}^{(2),\mathrm{GL}}(z_k)$ is given by eq 11. The total long-range correction energies $U_{\mathrm{LRC}}^{\mathrm{GL1}}$ and $U_{\mathrm{LRC}}^{\mathrm{GL12}}$, which are calculated by summing over all of the local contributions from each slab, are then added to the explicit configurational energy, U_{ST}, before and after an attempted atom displacement in the simulation. As a result, they affect the development of the Markov chain.

The local long-range corrections to the total energy within the kth slab are[19,24]

$$u_{\mathrm{lrc}}^{(1),\mathrm{GL}}(z_k) = \frac{8\pi}{3}\rho(z_k)^2 V_s \epsilon_{ij}\left[\left(\frac{\sigma^{12}}{3r_c^{9}}\right) - \left(\frac{\sigma^{6}}{r_c^{3}}\right)\right] \tag{10}$$

$$u_{\mathrm{lrc}}^{(2),\mathrm{GL}}(z_k) = \pi\rho(z_k)V_s\int_{r_c}^{\infty} \mathrm{d}r \int_{-r}^{r} \mathrm{d}\Delta z \sum_{i=1}^{N_z} [\rho(z_{k+i}) - \rho(z_{k+i-1})] r u_{\mathrm{LJ}}(r) \tag{11}$$

where $\rho(z_k)$ and V_s are respectively the density in and the volume of the kth slab. $\Delta z = z - z_k$, where Δz varies from $-r$ to r. N_z is the number of slabs between z and z_k. The first term is the same as the long-range correction for a spherical cutoff, r_c, in a homogeneous fluid of density $\rho(z_k)$. The second part is a double integral which contains a series of density differences which makes it cumbersome to calculate. Since the calculation of this term is time-consuming, it has been calculated *a posteriori* from configurations obtained with the truncated potential modified by the addition of $U_{\mathrm{LRC}}^{\mathrm{GL1}}$, and it has been suggested that it has little effect on the simulation results.[19,24]

In a second method, due to Janeček,

$$U_{\mathrm{ST}}^{\mathrm{JAN}} = \sum_{i=1}^{N-1}\sum_{j=i+1}^{N} u_{\mathrm{ST}}(r_{ij}) + U_{\mathrm{LRC}}^{\mathrm{JAN}} \tag{12}$$

where

$$U_{\mathrm{LRC}}^{\mathrm{JAN}} = \frac{1}{2}\sum_{k=1}^{N_s} u_{\mathrm{lrc}}^{\mathrm{JAN}}(z_k) \tag{13}$$

and the long-range correction energy of the slab k is

$$u_{\mathrm{lrc}}^{\mathrm{JAN}}(z_k) = \rho(z_k)V_s\sum_{j=1}^{N_s}\rho(z_j)\, w(|z_j - z_k|)\Delta z \tag{14}$$

where the sum is over all of the slabs in the box. The contribution $w(\xi) = w(|z_j - z_k|)$ is calculated by assuming a uniform distribution of atoms in the slab. For the Lennard-Jones potential, the function $w(\xi)$ is

$$w(\xi) = \begin{cases} 4\pi\epsilon\sigma^2\left[\frac{1}{5}\left(\frac{\sigma}{r_c}\right)^{10} - \frac{1}{2}\left(\frac{\sigma}{r_c}\right)^{4}\right] & \text{for } \xi \leq r_c \\ 4\pi\epsilon\sigma^2\left[\frac{1}{5}\left(\frac{\sigma}{\xi}\right)^{10} - \frac{1}{2}\left(\frac{\sigma}{\xi}\right)^{4}\right] & \text{for } \xi > r_c \end{cases} \tag{15}$$

Note that eq 13 defines the long-range correction energy as a sum over slabs whereas the original work[22] considers the correction in terms of a molecule i at z_i. Finally there is an improvement to the original version of Janeček's method proposed by MacDowell and Blas,[38] which avoids the decomposition of the long-range correction of the energy into local contributions and increases the speed of the calculation. We have used the original version of Janeček to facilitate a direct comparison with the method of Guo and Lu.

3. CALCULATION OF THE SURFACE TENSION

The intrinsic, or short-range, part of the surface tension, γ_I,[30] originally given by Kirkwood and Buff, is

DOI: 10.1021/acs.jctc.5b00377
J. Chem. Theory Comput. 2015, 11, 4573−4585

$$\gamma_I = \langle p_N - p_T \rangle L_z \tag{16}$$

where p_N and p_T are the normal and tangential components of the pressure and L_z is the length of the simulation cell in the z direction. Equation 16 is derived by differentiating the appropriate free energy with respect to surface area at constant volume. For the planar interface, p_N is given by p_{zz}, whereas the tangential component, p_T, is $(1/2)(p_{xx} + p_{yy})$. Since a two-phase simulation consists of two interfaces, the surface tensions calculated from eq 16 are divided by 2 to calculate γ for a single interface. The element $\alpha\beta$ of the configurational pressure tensor is

$$p_{\alpha\beta}^{\text{config}} = \frac{1}{V}\left\langle \sum_{i=1}^{N-1} \sum_{j=i+1}^{N} (\mathbf{r}_{ij})_\alpha (\mathbf{f}_{ij})_\beta \right\rangle \tag{17}$$

where α and β are the Cartesian coordinates, $\mathbf{r}_{ij} = \mathbf{r}_i - \mathbf{r}_j$, and $\mathbf{f}_{ij}$ is the intermolecular force between atoms i and j.

$$\mathbf{f}_{ij} = -\frac{\mathbf{r}_{ij}}{r_{ij}} \frac{\mathrm{d}u(r_{ij})}{\mathrm{d}r_{ij}} \tag{18}$$

where $u(r_{ij})$ refers to the $u_{\text{ST}}(r_{ij})$ and $u_{\text{STS}}(r_{ij})$ potential models. Trokhymchuk and Alejandre[11] have discussed the additional contribution in the force due to the discontinuity of the truncated potential at the cutoff distance. Since the pressure components and surface tensions are corrected by specific long-range corrections,[39] we do not consider this additional force in the calculation of these properties for simulations carried out with the truncated potential.

Irving and Kirkwood[30,39,45,46,53−56] have shown that γ_I can be calculated from $p_N(z)$ and $p_T(z)$, the components of the pressure tensor as a function of z;

$$\gamma_I = \int_{-L_z/2}^{L_z/2} (p_N(z) - p_T(z))\, \mathrm{d}z \tag{19}$$

Equation 19 is a mechanical definition of γ based upon the force acting across a unit area in the z-plane for one interface. There is no unique way of calculating the forces across a particular area, since it is unclear which atoms contribute to this force. This has no effect on $p_N(z)$, but different choices of the contour can affect the definition of $p_T(z)$. However, these choices have no effect on the integral in eq 19. A typical choice of contour[46,53,54] due to Irving and Kirkwood gives

$$p_{\alpha\beta}(z) = \langle \rho(z) \rangle k_B T \mathbf{I} + \frac{1}{A}\left\langle \sum_{i=1}^{N-1} \sum_{j=i+1}^{N} (\mathbf{r}_{ij})_\alpha (\mathbf{f}_{ij})_\beta \frac{1}{|z_{ij}|} \theta\left(\frac{z - z_i}{z_{ij}}\right) \theta\left(\frac{z_j - z}{z_{ij}}\right) \right\rangle \tag{20}$$

where $\mathbf{I}$ is the unit tensor and $\theta(x)$ is the unit step function defined as $\theta(x) = 0$ when $x < 0$ and $\theta(x) = 1$ when $x \geq 0$. A is the surface area and $\rho(z)$ is the local number density. The simulation box is divided into N_z slabs of thickness δz. Following Irving and Kirkwood, atoms i and j provide a contribution to the pressure tensor in a given slab if the line joining their centers crosses, starts, or finishes in the slab. The contribution to a particular slab is $1/|z_{ij}|$ of the ij interaction. Equation 19 is equivalent to eq 16. The advantage of the IK approach is that the profile of $p_N(z)$ is a constant for mechanical stability and combined with the symmetry of $p_T(z)$ around both interfaces provides a useful check of the accuracy of the simulation.

When simulations are performed using the truncated potentials of eqs 3, 6, 8, and 12, the long-range corrections to the surface tension are applied at the end of the simulation. For the truncated and shifted potential of eq 5, no long-range corrections are needed. The total surface tension γ sums the intrinsic part γ_I and the long-range correction part γ_{LRC}. Different expressions can be used to apply the long-range corrections to the surface tension.

The Fowler model uses $\rho(z) = \rho_l$ in the bulk liquid and $\rho(z) = 0$ in the bulk gas with a discontinuous change of density at the Gibbs dividing surface and gives

$$\gamma_{\text{LRC}}^{\text{FOW}} = \frac{\pi}{8}(\rho_l)^2 \int_{r_c}^{+\infty} \mathrm{d}r\, r^4 \frac{\mathrm{d}u_{\text{LJ}}(r)}{\mathrm{d}r} g(r) \tag{21}$$

Setting $g(r) = 1$ for large r and $\mathrm{d}u_{\text{LJ}}(r)/\mathrm{d}r \approx 24\epsilon\sigma^6/r^7$, we obtain

$$\gamma_{\text{LRC}}^{\text{FOW}} \approx \frac{3}{2}\pi\epsilon\sigma^6\left(\frac{\rho_l}{r_c}\right)^2 \tag{22}$$

Starting from the expression of Kirkwood−Buff,[30] Chapela et al.[3] suggested a model in which $\rho(z)$ is fitted to a hyperbolic tangent function of width d.

$$\rho(z) = \frac{1}{2}(\rho_l + \rho_g) - \frac{1}{2}(\rho_l - \rho_g)\tanh(2(z - z_g)/d) \tag{23}$$

where z_g is the position of the Gibbs dividing surface. The resulting expression, corrected later by Blokhuis et al.,[18] is

$$\gamma_{\text{LRC}}^{\text{BLO}} = \frac{\pi}{2}(\rho_l - \rho_v)^2 \int_0^1 \mathrm{d}s \int_{r_c}^{+\infty} \mathrm{d}r \coth\left(\frac{2rs}{d}\right) \frac{\mathrm{d}u_{\text{LJ}}(r)}{\mathrm{d}r} r^4(3s^3 - s) \tag{24}$$

The long-range corrections to the pressure tensor in a particular slab, k, in the Guo and Lu approach[19] are

$$\begin{aligned} p_{N,\text{lrc}}^{\text{GL}}(z_k) &= p_{N,\text{lrc}}^{(1),\text{GL}}(z_k) + p_{N,\text{lrc}}^{(2),\text{GL}}(z_k) \\ &= -\frac{2\pi}{3}\rho^2(z_k) \int_{r_c}^{\infty} \mathrm{d}r\, r^3 \frac{\mathrm{d}u_{\text{LJ}}(r)}{\mathrm{d}r} \\ &\quad - \pi\rho(z_k) \int_{r_c}^{\infty} \mathrm{d}r \int_{-r}^{r} \mathrm{d}\Delta z \frac{\mathrm{d}u_{\text{LJ}}(r)}{\mathrm{d}r} \\ &\quad \times \sum_{i=1}^{N_c} [\rho(z_{k+i}) - \rho(z_{k+i-1})](\Delta z)^2 \end{aligned} \tag{25}$$

$$\begin{aligned} p_{T,\text{lrc}}^{\text{GL}}(z_k) &= p_{T,\text{lrc}}^{(1),\text{GL}}(z_k) + p_{T,\text{lrc}}^{(2),\text{GL}}(z_k) \\ &= -\frac{2\pi}{3}\rho^2(z_k) \int_{r_c}^{\infty} \mathrm{d}r\, r^3 \frac{\mathrm{d}u_{\text{LJ}}(r)}{\mathrm{d}r} \\ &\quad - \frac{\pi}{2}\rho(z_k) \int_{r_c}^{\infty} \mathrm{d}r \int_{-r}^{r} \mathrm{d}\Delta z \frac{\mathrm{d}u_{\text{LJ}}(r)}{\mathrm{d}r} \\ &\quad \times \sum_{i=1}^{N_c} [\rho(z_{k+i}) - \rho(z_{k+i-1})][r^2 - (\Delta z)^2] \end{aligned} \tag{26}$$

From these expressions, the LRC to the surface tension is obtained from the pressure tensor as

DOI: 10.1021/acs.jctc.5b00377
J. Chem. Theory Comput. 2015, 11, 4573−4585

$$\gamma_{\mathrm{lrc}}^{\mathrm{GL}}(z_k) = \frac{V_s}{A}(p_{N,\mathrm{lrc}}^{(2),\mathrm{GL}}(z_k) - p_{T,\mathrm{lrc}}^{(2),\mathrm{GL}}(z_k)) = \frac{\pi}{2}\rho(z_k)\frac{V_s}{A}\int_{r_c}^{\infty} \mathrm{d}r \int_{-r}^{r} \mathrm{d}\Delta z \frac{\mathrm{d}u_{\mathrm{LJ}}(r)}{\mathrm{d}r} \times \sum_{i=1}^{N_s} [\rho(z_{k+i}) - \rho(z_{k+i-1})][r^2 - 3(\Delta z)^2] \quad (27)$$

The total long-range correction $\gamma_{\mathrm{LRC}}^{\mathrm{GL}}$ to the surface tension is obtained by summing the local contributions $\gamma_{\mathrm{lrc}}^{\mathrm{GL}}(z_k)$ of each bin and dividing the result by a factor 2.

With the Janeček approach, the normal and tangential components of the long-range corrections of the pressure tensor are

$$p_{N,\mathrm{lrc}}^{\mathrm{JAN}}(z_k) = \rho(z_k)\sum_{j=1}^{N_s}\rho(z_j)\,\pi_{zz}(|z_j - z_k|)\,\Delta z \quad (28)$$

$$p_{T,\mathrm{lrc}}^{\mathrm{JAN}}(z_k) = \frac{1}{2}(p_{xx,\mathrm{lrc}}^{\mathrm{JAN}}(z_k) + p_{yy,\mathrm{lrc}}^{\mathrm{JAN}}(z_k)) = \rho(z_k)\sum_{j=1}^{N_s}\rho(z_j)\frac{1}{2}(\pi_{xx}(|z_j - z_k|) + \pi_{yy}(|z_j - z_k|))\,\Delta z \quad (29)$$

In eqs 28 and 29, the functions $\pi_{xx}(\xi)$, $\pi_{yy}(\xi)$, and $\pi_{zz}(\xi)$ are given by

$$\pi_{xx}(\xi) = \pi_{yy}(\xi) = \begin{cases} 2\pi\epsilon\left[\frac{6r_c^2 - 5\xi^2}{5}\left(\frac{\sigma}{r_c}\right)^{12} - \frac{3r_c^2 - 2\xi^2}{2}\left(\frac{\sigma}{r_c}\right)^{6}\right] & \text{for } \xi \le r_c \\ 2\pi\epsilon\left[\frac{\xi^2}{5}\left(\frac{\sigma}{\xi}\right)^{12} - \frac{\xi^2}{2}\left(\frac{\sigma}{\xi}\right)^{6}\right] & \text{for } \xi > r_c \end{cases} \quad (30)$$

$$\pi_{zz}(\xi) = \begin{cases} 4\pi\epsilon\xi^2\left[\left(\frac{\sigma}{r_c}\right)^{12} - \left(\frac{\sigma}{r_c}\right)^{6}\right] & \text{for } \xi \le r_c \\ 4\pi\epsilon\xi^2\left[\left(\frac{\sigma}{\xi}\right)^{12} - \left(\frac{\sigma}{\xi}\right)^{6}\right] & \text{for } \xi > r_c \end{cases} \quad (31)$$

Finally

$$\gamma_{\mathrm{lrc}}^{\mathrm{JAN}}(z_k) = \frac{V_s}{A}[p_{N,\mathrm{lrc}}^{\mathrm{JAN}}(z_k) - p_{T,\mathrm{lrc}}^{\mathrm{JAN}}(z_k)] \quad (32)$$

The total long-range correction $\gamma_{\mathrm{LRC}}^{\mathrm{JAN}}$ to the surface tension using the Janeček methodology is then calculated by summing the local contributions $\gamma_{\mathrm{lrc}}^{\mathrm{JAN}}(z_k)$ of each bin and dividing the result $\gamma_{\mathrm{LRC}}^{\mathrm{JAN}}$ by a factor of 2 to account for the two planar interfaces in the box.

4. SIMULATION DETAILS

The initial configuration was constructed by placing N atoms in an orthorhombic box of 50 × 50 × 130 Å^3. The number of atoms N = 5000 and the initial volume were chosen to create the coexisting liquid density, ρ_l, at 100 and 125 K. MC simulations in the constant-NVT ensemble were performed on this single-phase liquid configuration. The dimension of the initial box was increased along the z-axis by placing two empty cells on either side of the original box. The resulting two-phase simulation box was rectangular with a volume $V = L_xL_yL_z$ and an interfacial area defined by $A = L_xL_y$. The periodic boundary conditions were applied to the extended box in all three directions. The dimensions of the cell are $L_x = L_y$ = 50 Å = 13.4 σ while L_z = 300 Å = 80.4 σ. These dimensions are significantly larger than those recommended[9,11] to avoid any dependence of the surface tension on the system size.

MC simulations were performed in the constant-NVT ensemble. All simulations were organized in cycles. Each cycle consisted of N translations of the atoms. The equilibration phase was composed of 500000 cycles and the production phase of 2 × 10^6 cycles (10^{10} translation moves). The maximum displacement was adjusted during the equilibrium phase to give an acceptance ratio of 0.4. The thermodynamic interfacial properties were calculated every 20 cycles requiring the storage of 100000 configurations. The statistical errors for these properties were estimated using five superblocks averages of 20000 configurations.

The long-range corrections to the energy are applied at **each** MC move although the density profile used to calculate the long-range corrections is updated every 10 MC cycles[23] and is calculated with a slab thickness δz of 0.5 Å. To test this approach, we reduced the frequency for the update of the density profile to a single MC cycle and we did not observe any change in the profiles of the tail energy once the equilibrium had been reached. We have used a frequency of 10 MC cycles for the density update as a good compromise between the computational cost of the update and an accurate calculation of the long-range properties.

The detailed MC calculations were carried out at two temperatures, T = 100 K (T^* = 0.667) and T = 125 K (T^* = 0.834). Additional temperatures in the range 100−175 K were studied to obtain the phase diagram and to compare the Guo and Lu and Janeček corrections on the phase diagram. To allow a direct comparison of our results with the various studies of the Lennard-Jones liquid−vapor interface, we have reported our results using both the dimensionless reduced quantities indicated by an asterisk and the real units related through the following expressions:[26] $T^* = k_BT/\epsilon$, $\gamma^* = \gamma\sigma^2/\epsilon$, $L^* = L/\sigma$, $U^* = U/\epsilon$, $P^* = P\sigma^3/\epsilon$, and $\rho^* = \rho\sigma^3$ where T^*, γ^*, L^*, U^*, P^*, and ρ^* represent the reduced temperature, surface tension, length, energy, pressure, and density, respectively. We used the LJ parameters for the methane molecule.[52]

The Monte Carlo simulations were carried out on a parallel architecture formed from 12 processors. The list of interacting particles is split equally between the processors at each move. We did not consider a domain decomposition since the box length along the x and y directions is small compared to the cutoff radius. The computational time for these simulations ranges then from 3 to 8 days depending on the value of the cutoff radius used and on the method used to include the long-range corrections to the energy into the simulation.

5. RESULTS AND DISCUSSIONS

5.1. Methodological Issues. Since simulations of two-phase systems are sensitive to size-effects,[9,56,57] we use a large enough box, in both the perpendicular and lateral directions, to avoid the size dependence of the interfacial properties. Figure 2 shows the density profiles calculated along the normal to the surface at different temperatures for a truncated LJ potential using a cutoff r_c = 3.2 σ = 12 Å. In the range of temperature 100−175 K, the density profiles show well-developed liquid and

DOI: 10.1021/acs.jctc.5b00377
J. Chem. Theory Comput. 2015, 11, 4573−4585

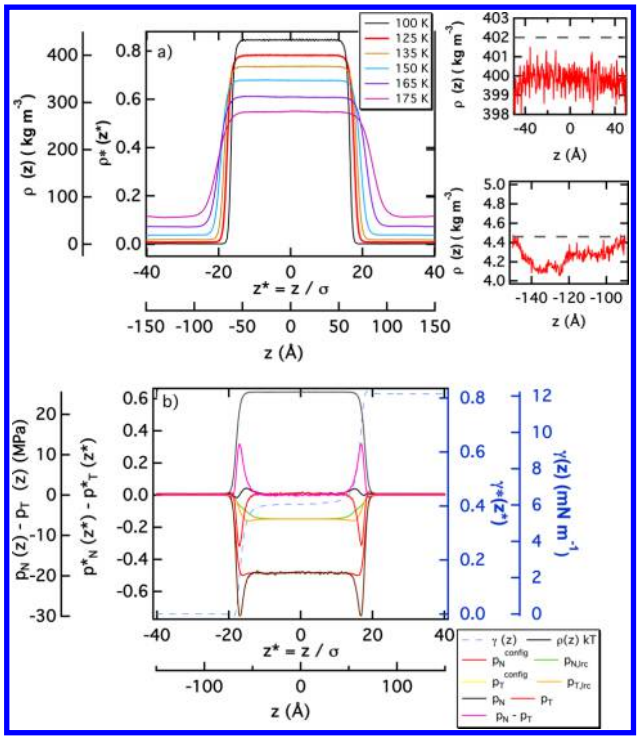

Figure 2. (a) Density profiles along the normal to the surface calculated in a simulation carried out with the LJ potential truncated at r_c = 3.2 σ = 12 Å in the temperature range of 100−175 K. The insets focus on the bulk liquid and gas phases at 125 K where the dashed lines represent the experimental values. (b) Profiles of the different contributions to the normal and tangential pressure components calculated at T = 125 K obtained from the LJ truncated potential with r_c = 3.2 σ. We report the profiles of the ideal term $\langle\rho(z)k_BT\rangle$ (see eq 20), the long-range corrections parts calculated using the Janeček method (see eqs 28 and 29), the configurational part calculated using the second term of eq 20, and the total pressure that sums all of these contributions. The profile of the integral $\gamma(z) = (1/2)\int_{-L_z/2}^{z} (p_N(z) - p_T(z))\, dz$ is represented on the right-hand axis. The final value of the profile is that of the surface tension.

vapor phases. We note that T = 100 K is above the triple point of methane T_T = 90 K that is slightly below the triple point of the LJ fluid. We see no sign of the formation of a solid−vapor equilibrium as evidenced by the smooth density profile in Figure 2. At T = 125 K, the profile shows a liquid phase extending over 100 Å with two vapor phases of 75 Å on each side. The two insets, focusing on liquid and vapor phases at 125 K, establish a liquid density of ρ_l = 399 ± 1 kg m^{-3} and a vapor density of ρ_v = 4.3 ± 0.1 kg m^{-3} leading to deviations from experimental results for coexisting methane of 0.7% and 2%, respectively. More importantly, the box size and the length of the production phase are long enough to obtain reliable coexisting densities with statistical fluctuations of the order of 0.5% and 2% for the liquid and vapor densities demonstrating that these calculations are fully converged.

Figure 2b shows the profiles of the different contributions to the normal and tangential components of the pressure tensor calculated at 125 K for the truncated ST potential: the ideal part defined by $\langle\rho(z)k_BT\rangle$, the configurational contribution represented by the second term in eq 20, the long-range corrections to the pressure calculated by the Janeček method using eqs 28 and 29, and the sum of these contributions in the $p_N(z)$ and $p_T(z)$ local components. The main features of the mechanical equilibrium for a planar liquid−vapor interface is satisfied for all of the contributions: $p_T(z) = p_N(z)$ in the bulk vapor and liquid phases and a negative peak of the tangential component of the configurational part to the pressure in the interfacial region. We also note that the contribution of the long-range corrections to the pressure in the liquid phase represents 40% of the configurational part for r_c = 3.2 σ. The profiles of the total component of the normal and tangential pressure components are in line with both those expected by a planar interface at equilibrium and those calculated from MC and MD simulations.[39,56] The profile of the difference between the normal and tangential pressure profiles shows two symmetric peaks at the interfaces with no contribution in the bulk phases. The integral of this profile $\gamma(z) = (1/2)\int_{-L_z/2}^{z} (p_N(z) - p_T(z))\, dz$ is plotted on the right axis. As expected, the profile of $\gamma(z)$ is constant in the bulk phases and the contributions from both interfaces are the same.

To allow a direct comparison between the profiles of the local configurational energy and the pressure components calculated using both the Guo and Lu and the Janeček methods, we generate a sequence of configurations using the truncated LJ potential at r_c = 3.2 σ at T = 125 K (no tail corrections are included in the Metropolis scheme). This approach enables us to evaluate different approximate corrections applied to *exactly* the same set of configurations and hence to evaluate the accuracy of the methods.

Figure 3 shows the profiles of the first and second terms of the Guo and Lu tail corrections for the configurational energy

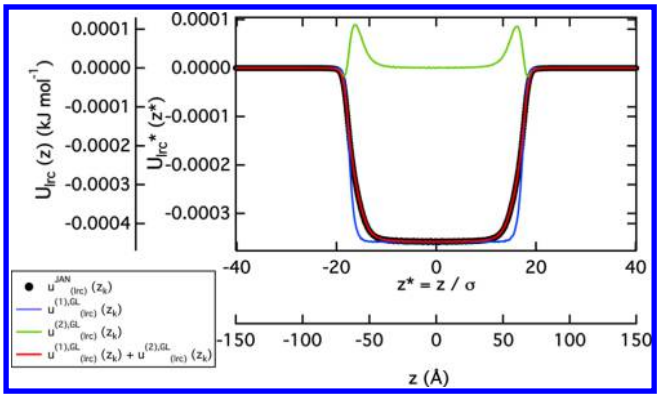

Figure 3. Profiles of the first and second terms of the tail corrections of the configurational energy calculated with the Guo and Lu method using eqs 10 and 11. The profile of the LRC to the configurational energy calculated with the Janeček method with eq 14 is also reported for comparison. All of these LRCs contributions are calculated over configurations obtained using the truncated LJ potential at r_c = 12 Å and T = 125 K. These LRCs profiles are normalized by the total number of particles N = 5000.

as a function of z. The second contribution to the energy exhibits two positive peaks in the interface region with smaller negative values on the vapor side of the interface. These features are in line with those reported by the original work of Guo and Lu.[19] This contribution is significantly smaller than the first term, but it does contribute in the interfacial region. The full versions of the Guo and Lu method and the Janeček method give profiles of the tail corrections to the configurational energy in perfect agreement. The use of only the first term creates an error of ca. 5% in the calculation of the local potential energy.

DOI: 10.1021/acs.jctc.5b00377
J. Chem. Theory Comput. 2015, 11, 4573−4585

Figure 4a shows the profiles of the difference between the long-range corrections of the normal and tangential pressure

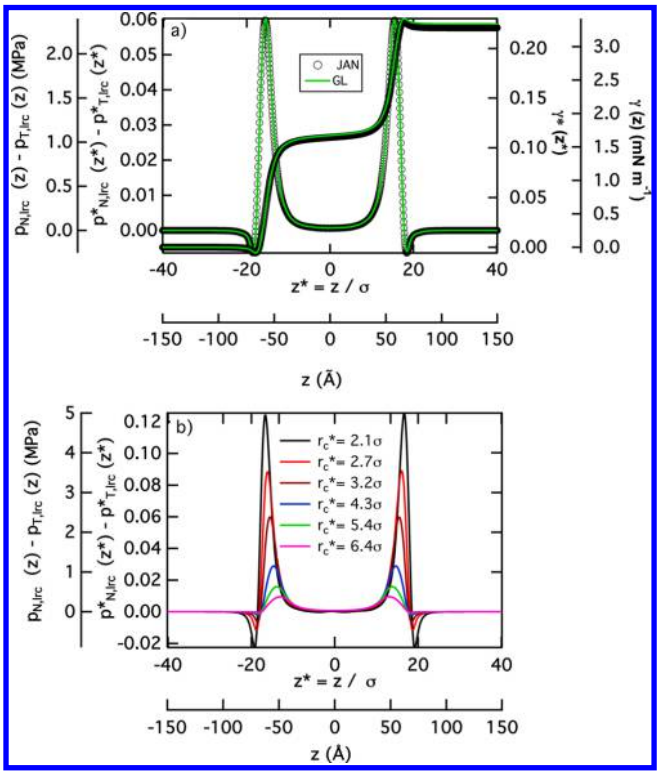

Figure 4. (a) Profiles of the difference between the long-range corrections to the normal and tangential pressure components calculated using both slab-based tail corrections methodologies with eqs 25 and 26 for the Guo and Lu method and eqs 28 and 29 with the Janeček method. The configurations were generated by using the truncated LJ potential at r_c = 12 Å at T = 125 K. (b) Profiles of ($p^{JAN}_{N,lrc}$−$p^{JAN}_{T,lrc}$) calculated with the Janeček method at different cutoff values.

components calculated with the Guo and Lu method using eqs 25 and 26 and with the Janeček method using eqs 28 and 29. The corresponding integrals are also plotted for completeness. The comparison shows that the two slab-based tail corrections methods give identical profiles of the long-range corrections for the normal and tangential pressure components. The integrals resulting from these profiles are also shown in Figure 4a and are indistinguishable.

The value of the tail correction of the surface tension calculated from the profiles is 0.224 (3.33 mN m^{-1}) for the method of Guo and Lu and 0.221 (3.28 mN m^{-1}) for that of Janeček (see also Table 1). The tail contributions to the surface tension differ by only 1.5% establishing the equivalence of the two tail expressions for the surface tension over the same set of configurations. This equivalence of the two slab-based tail corrections methods is demonstrated in Table 1 for different cutoff radii at two different temperatures. The maximum deviation between the Guo and Lu method and the Janeček method does not exceed 5%.

The values of the long-range corrections to the surface tension calculated from the expressions established by Fowler (see eq 22) and by Blokhuis (see eq 24) are included in Table 1 for comparison. As expected, the tail correction deduced from the Fowler expression is inaccurate and differs significantly from the other expressions particularly as the vapor density and the interfacial thickness are no longer negligible. The tail values

Table 1. Values of Surface Tensions (Intrinsic and Long-Range Corrections Contributions) Calculated from Configurations Obtained with the LJ Potential Truncated at r_c = 12 Å at T = 100 K and T = 125 K[a]

r_c*	γ_I*	(γ^{FOW}_{LRC})*	(γ^{BLO}_{LRC})*	(γ^{JAN}_{LRC})*	(γ^{GL}_{LRC})*
		T* = 0.6670			
2.14	0.518_{24}	0.693	0.555	0.542	0.565
2.41	0.698_{24}	0.559	0.474	0.465	0.480
2.68	0.792_{9}	0.456	0.398	0.393	0.402
3.21	0.923_{9}	0.327	0.296	0.293	0.297
3.75	1.000_{27}	0.241	0.224	0.222	0.224
4.29	1.050_{23}	0.186	0.175	0.174	0.175
4.82	1.101_{24}	0.148	0.140	0.139	0.140
5.36	1.113_{27}	0.120	0.114	0.114	0.114
6.43	1.164_{18}	0.083	0.080	0.080	0.080
		T* = 0.8338			
2.14	0.301_{12}	0.548	0.356	0.346	0.365
2.41	0.424_{16}	0.456	0.332	0.326	0.339
2.68	0.503_{10}	0.374	0.288	0.284	0.292
3.21	0.595_{11}	0.270	0.222	0.221	0.225
3.75	0.672_{15}	0.201	0.173	0.172	0.173
4.29	0.719_{7}	0.155	0.137	0.137	0.137
4.82	0.741_{7}	0.123	0.110	0.110	0.111
5.36	0.759_{13}	0.100	0.091	0.091	0.091
6.43	0.790_{5}	0.070	0.064	0.064	0.064
r_c	γ_I	γ^{FOW}_{LRC}	γ^{BLO}_{LRC}	γ^{JAN}_{LRC}	γ^{GL}_{LRC}
		T = 100 K			
8.0	7.7_{3}	10.3	8.2	8.1	8.4
12.0	13.7_{1}	4.8	4.4	4.3	4.4
14.0	14.9_{4}	3.6	3.3	3.3	3.3
24.0	17.3_{3}	1.2	1.2	1.2	1.2
		T = 125 K			
8.0	4.5_{2}	8.1	5.3	5.1	5.4
12.0	8.8_{2}	4.0	3.3	3.3	3.3
14.0	10.0_{2}	3.0	2.6	2.5	2.6
24.0	11.7_{1}	1.0	0.95	0.95	0.95

[a]The long-range corrections to the surface tension are calculated from different expressions described in Section 3. We also provide values in real units for some cutoff values: γ (mN m^{-1}) and r_c (Å). The subscripts give the accuracy of the last decimal places, *i.e.*, 0.518_{24} means 0.518 ± 0.024.

calculated from the expression of Blokhuis are between those calculated from the Guo and Lu and Janeček methods. The cutoff dependence of the profiles of the long-range corrections to the surface tension calculated from the Janeček method is shown in Figure 4b. The long-range corrections to the surface tension range from 50% of the total value to 7% in the 2.1−6.4 σ over the cutoff range considered. Even with a large cutoff of r_c = 6.4 σ = 24 Å, we observe a non-negligible tail contribution in the interface region. In addition, the system size used here allows one to reproduce local tail contributions that approach zero in the bulk liquid and vapor phases. Such profiles are required to check the consistency of the methodology used for the modeling of the two-phase simulation.

To conclude this section, the expressions developed by Guo and Lu give the same tail corrections for the surface tension as those obtained with the Janeček method applied to the same set of configurations. The Fowler-type corrections do not produce accurate results for the truncated potential model. Interestingly the Blokhuis correction converges to the Guo and Lu and Janeček corrections at larger cutoffs (from r_c> 3.8 σ).

DOI: 10.1021/acs.jctc.5b00377
J. Chem. Theory Comput. 2015, 11, 4573−4585

5.2. Cutoff Dependence of the Surface Tension. The total surface tension defined by the sum of the intrinsic (γ_I) and long-range (γ_{LRC}) corrections contributions is shown as a function of the cutoff in Figure 5 for the different potential

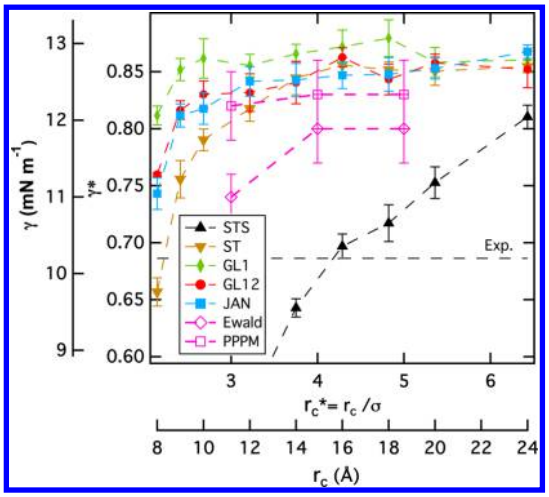

Figure 5. Surface tension values as a function of the cutoff distance calculated with different potential models at 125 K. The potential models are indicated in the legend. The experimental value[58] is shown for completeness. The surface tensions calculated with the Ewald and PPPM methods are taken from ref 49.

models at T = 125 K. When the truncated LJ potential U_{ST} is used, no long-range corrections are applied to the configurational energy and the surface tension is then corrected by using only the tail contribution of Blokhuis (eq 24) calculated from the density profile $\rho(z)$. When the truncated and shifted potential U_{STS} is used in the Monte Carlo simulation, no long-range corrections are applied to the surface tension. We also report the simulated surface tensions for the GL1, GL12, and JAN corrections when they are included directly in the Metropolis criterion. Table 2 summarizes the values of the surface tensions at T = 100 K and T = 125 K including the intrinsic and tail contributions. To illustrate the size of these effects, we provide the values of surface tension in SI units for some of the cutoff values considered. We also report in Figure 5 the surface tensions calculated from MD simulations[49] of the LJ fluid at T = 127 K using the Ewald and PPPM methods for the calculation of the dispersion interactions.

First, when the full tail energy correction developed by Guo and Lu (GL12) is used to drive the trajectories, the dependence of the surface tension on the cutoff radius is identical to that calculated when the Janeček method is used. Within the cutoff range of r_c = 2.1−6.4 σ, the surface tension calculated by the two slab-based tail correction methods increases by 12%. From a cutoff of r_c = 3.2 σ (12 Å), corresponding to the smallest cutoff used in the most current simulations, there is no cutoff dependence for the surface tension within the statistical fluctuations. This is in line with recent simulations[25] carried out with the Janeček tail correction. Second, when only the first term of Guo and Lu is applied in the simulation (GL1), we observe a 2% overestimate of γ in the cutoff range 2.5−5 σ and a correspondence with the limiting value calculated with the method of Janeček for a cutoff greater than r_c = 5 σ. It is worth recalling that, in terms of real units, GL1 is overestimating the surface tension by only 0.4 mN m^{-1}. The magnitude of this deviation is close to the statistical fluctuations normally observed for the simulation of the surface tension. Third, the use of the pure truncated potential, U_{ST}, leads to a strong dependence of the surface tension on the cutoff in the range of 2.1−4 σ with an increase of γ of 25%. Working with the truncated potential in two-phase simulations requires a cutoff value from at least 4 σ (14 Å). However, once r_c > 4 σ, the use of the U_{ST} with the *a posteriori* application of the Blokhuis correction produces results for the surface tension that are as accurate as the application of the Janeček method applied at each step of the simulation. When the dispersion interactions are calculated with the Ewald and PPPM methods,[49] a dependence of the surface tension on the cutoff is observed with the Ewald method for cutoff values smaller than r_c = 4 σ and no dependence is seen with the PPPM method. The surface tensions calculated with these two methods match very well those calculated with GL12 and JAN within the statistical fluctuations.

Finally, the use of the truncated and shifted potential U_{STS} leads to a monotonic increase of the surface tension with the cutoff without reaching the limiting value obtained with the other potentials in the cutoff range investigated here. Actually, in addition to the values of σ and ϵ, the U_{STS} potential contains a third adjustable parameter, the cutoff. Any agreement obtained with experiment using this model is fortuitous, and this potential with three adjustable parameters cannot give quantitative predictions of the surface tension due to its lack of transferability.

It is clear that all of the other methods that accurately apply a long-range correction overestimate the *experimental* surface tension by ca. 21%.[58] It is unlikely that these differences arise from the neglect of the weak permanent-electrostatic interaction or from the three-body terms[44,59,60] in the interaction potential since the polarizability is small. The difference may be attributed to the fact that the LJ potential does not accurately account for the dispersion interaction in methane and that the interaction parameters were not fitted to the experimental surface tension as a target property.

It is useful to breakdown the variations in total surface tension into the intrinsic and LRC contributions. These two contributions are shown in Figure 6a,b. Apart from the truncated and shifted potential, the intrinsic contributions γ_I to the surface tension are close for all of the models considered. This is an important conclusion because in calculating the surface tension, we can avoid the inclusion of the long-range corrections in the underlying simulation and simply work with U_{ST}.

There are differences in the different potential models for the long-range contribution at small cutoffs, and this is shown in Figure 6b. The long-range corrections to the surface tension calculated from the truncated potentials with the Blokhuis expression are significantly smaller than those calculated by the slab-based tail corrections methods for r_c < 4 σ. Note that when the long-range corrections to the surface tensions are calculated on the same configurations (see Table 1), the method of Blokhuis overestimates this correction as compared to the Janeček method. When we move to higher temperatures on the phase diagram, the ratio of the long-range corrections to the total surface tension is slightly higher (from 28% to 35% for r_c = 3.2 σ). The same dependence on cutoff is expected at higher temperatures. It is clear that the accurate calculation of the Blokhuis correction requires an accurate estimate of the coexisting densities, and we examine this problem in the next section.

DOI: 10.1021/acs.jctc.5b00377
J. Chem. Theory Comput. 2015, 11, 4573−4585

Table 2. Long-Range Corrections and Total Surface Tension Values Calculated at Different Cutoff Distances with Different Potential Models U_{ST}, U_{STS}, U_{ST}^{GL1}, U_{ST}^{GL12}, and U_{ST}^{JAN} Defined in Equations 2, 4, 6, 8, and 12, Respectively[a]

	U_{STS}		U_{ST}		U_{ST}^{GL1}		U_{ST}^{GL12}		U_{ST}^{JAN}	
r_c^*	γ_{LRC}^*	γ^*	$(\gamma_{LRC}^{BLO})^*$	γ^*	$(\gamma_{LRC}^{GL})^*$	γ^*	$(\gamma_{LRC}^{GL})^*$	γ^*	$(\gamma_{LRC}^{JAN})^*$	γ^*
					$T^* = 0.667$					
2.14	0	0.41_1	0.55	1.07_2	0.64	1.20_1	0.61	1.16_1	0.58	1.14_2
2.41	0	0.59_1	0.47	1.17_1	0.51	1.25_1	0.50	1.23_1	0.48	1.21_1
2.67	0	0.72_2	0.40	1.19_1	0.42	1.25_1	0.41	1.23_2	0.40	1.21_1
3.21	0	0.88_1	0.30	1.21_1	0.30	1.24_1	0.30	1.22_2	0.30	1.23_1
3.75	0	0.98_1	0.22	1.22_1	0.23	1.24_2	0.22	1.23_2	0.22	1.24_1
4.29	0	1.06_1	0.17	1.23_1	0.18	1.25_2	0.17	1.23_2	0.17	1.24_1
4.82	0	1.09_1	0.14	1.24_1	0.14	1.24_2	0.14	1.24_2	0.14	1.23_1
5.36	0	1.13_1	0.11	1.24_1	0.11	1.24_2	0.11	1.23_3	0.11	1.23_2
6.43	0	1.16_2	0.079	1.24_1	0.079	1.24_2	0.079	1.23_3	0.079	1.23_2
					$T^* = 0.834$					
2.14	0	0.15_1	0.36	0.66_1	0.46	0.81_1	0.42	0.76_1	0.41	0.74_1
2.41	0	0.30_1	0.33	0.75_1	0.38	0.85_1	0.36	0.82_1	0.35	0.81_1
2.67	0	0.42_2	0.29	0.79_1	0.32	0.86_2	0.31	0.83_1	0.30	0.82_1
3.21	0	0.56_1	0.22	0.82_1	0.23	0.85_1	0.23	0.83_2	0.23	0.84_1
3.75	0	0.64_1	0.17	0.84_1	0.18	0.86_1	0.17	0.84_2	0.18	0.84_1
4.29	0	0.70_1	0.14	0.85_1	0.14	0.87_1	0.14	0.86_1	0.14	0.85_1
4.82	0	0.72_1	0.11	0.85_1	0.11	0.88_2	0.11	0.84_1	0.11	0.85_1
5.36	0	0.75_1	0.091	0.85_1	0.091	0.86_1	0.091	0.86_1	0.091	0.85_1
6.43	0	0.81_1	0.064	0.85_1	0.064	0.86_1	0.064	0.85_2	0.064	0.87_1
	U_{STS}		U_{ST}		U_{ST}^{GL1}		U_{ST}^{GL12}		U_{ST}^{JAN}	
r_c	γ_{LRC}	γ	γ_{LRC}^{BLO}	γ	γ_{LRC}^{GL}	γ	γ_{LRC}^{GL}	γ	γ_{LRC}^{JAN}	γ
					$T = 100$ K					
8.0	0	6.1_1	8.2	15.9_4	9.5	17.8_2	8.2	17.2_5	8.7	16.9_3
12.0	0	13.0_1	4.4	18.1_4	4.5	18.4_2	4.5	18.2_4	4.4	18.3_1
14.0	0	14.6_2	3.5	18.2_4	3.4	18.4_2	3.3	18.2_3	3.3	18.4_2
24.0	0	17.2_4	1.2	18.5_2	1.2	18.4_3	1.2	18.4_3	1.2	18.4_3
					$T = 125$ K					
8.0	0	2.2_1	5.3	9.7_2	6.8	12.0_1	6.3	11.3_1	6.0	11.0_2
12.0	0	8.3_1	3.3	12.1_2	3.5	12.7_1	3.4	12.3_2	3.4	12.5_2
14.0	0	9.5_1	2.6	12.5_2	2.6	12.8_1	2.6	12.5_2	2.6	12.5_2
24.0	0	12.0_1	0.95	12.7_1	0.95	12.8_1	0.95	12.7_2	0.95	12.9_1

[a]The surface tensions γ^* are given in reduced units, and the values of γ in mN m^{-1}. The total γ^* sums the intrinsic part γ_I^* and the long-range part γ_{LRC}^*. The cutoff radius r_c is given in Å. The subscripts give the accuracy of the last decimal(s); *i.e.*, 1.20_1 means 1.20 ± 0.01.

5.3. Cutoff Dependence of the Coexisting Densities. Figure 7 shows a strong dependence of the liquid and vapor densities on the cutoff radius for the truncated potentials (U_{ST} and U_{STS}). The dependence is weaker for the methods using the tail corrections to the energy directly in the simulation. For the GL1, GL12, and JAN methods, the dependence on cutoff is smaller than the statistical fluctuations for $r_c > 4.0\ \sigma$. The trend of the liquid and vapor densities with the increasing cutoff radius is identical for each of the three slab-based tail corrections methods. We note that the prediction of the coexisting densities is the same for GL1 and GL12. The liquid densities calculated from the Ewald and PPPM dispersion methods[49] exhibit no dependence on the cutoff. The deviations between these liquid densities and those calculated by GL12 and JAN are less than 1%.

The reason for the underestimate in the long-range corrections to the surface tension calculated by the method of Blokhuis (see Figure 6b) is clear. This correction contains a term in $(\rho_l - \rho_v)^2$, and from Figure 7, we see that the liquid density is too low at cutoff distances less than $3.5\ \sigma$. The impact of inaccuracy in the coexisting densities on the surface tension is relatively weak. Actually, for $T = 125$ K, changing the value of $(\rho_l - \rho_v)^2$ calculated at $r_c = 3\ \sigma$ in γ_{LRC}^{BLO} to the converged value at $r_c = 6.43\ \sigma$ amounts to a change of the long-range corrections to γ of only 0.01 in reduced units or 0.15 mN m^{-1}. This small difference is within the statistical fluctuations of the surface tension calculation and explains why the surface tension converges for cutoff values smaller than the liquid and vapor densities.

To investigate the temperature dependence of the simulated coexisting densities, we report in Figure 8a the phase diagram of the methane in the temperature range 100−175 K determined with the truncated (ST) potential and the JAN and GL methods. The simulations were performed using $r_c = 3.2\ \sigma$. We observe that the GL and JAN methods perform equally well in reproducing the liquid and vapor densities over the whole coexistence curve. A crude prediction of the critical point can be made using the law of the rectilinear diameters. In this case, the prediction of the critical temperature by using JAN and GL is within 1% of experiments and the critical density is estimated within 1.5% of experiments. In Figure 8b we present the vapor pressure as a function of the inverse temperature. The simulated vapor pressures match the experimental pressures regardless of the method used. We

DOI: 10.1021/acs.jctc.5b00377
J. Chem. Theory Comput. 2015, 11, 4573−4585

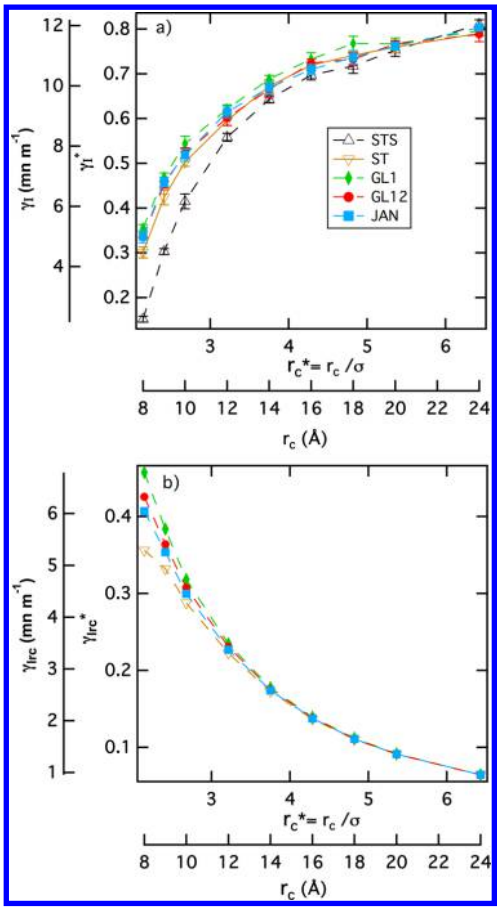

Figure 6. (a) Intrinsic and (b) long-range corrections parts of the surface tension as a function of the cutoff for different potential models as indicated in the legend at T = 125 K.

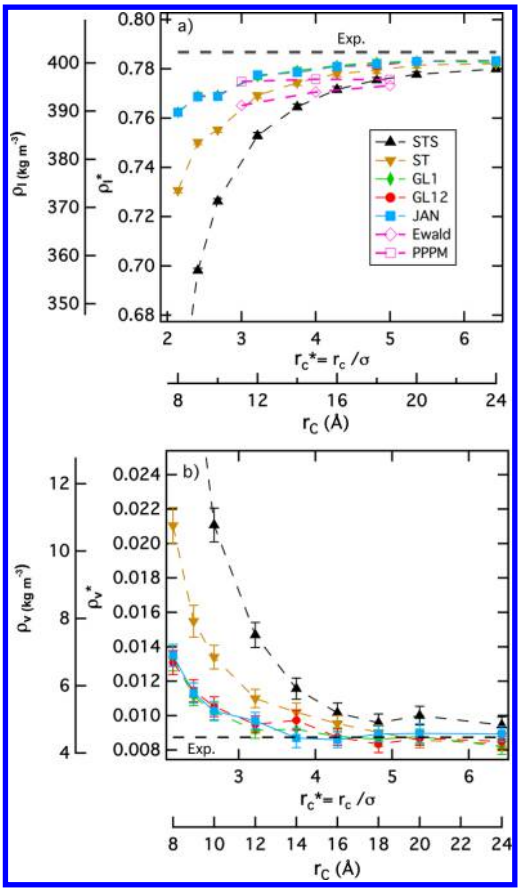

Figure 7. Calculated (a) liquid (ρ_l) and (b) vapor (ρ_v) densities of the coexisting phases as a function of the cutoff at 125 K. The different potential models are indicated in the legend. The experimental densities[58] are shown for comparison. The liquid densities calculated from MD simulations using the Ewald and PPPM methods can be found in ref 49.

observe a slight overestimation of the vapor pressure calculated with the truncated (ST) LJ potential in line with overestimated vapor densities. In contrast to the surface tension, the simulated coexisting densities and vapor pressures are close to the experimental values.[58] The parametrization procedure of the LJ potential includes these experimental data.

5.4. Timings. Figure 9 shows the relative running time of the simulations using the ST potential and the JAN and GL methods as a function of the cutoff value. The linear scaling of the simulation time with r_c is expected for the use of a link-cell method. The steep rises in the curve at 2.5 σ and 3.5 σ are a result of the inefficiencies of the link-cell method associated with the change in r_c for relatively small box sizes. The timings presented are relative to a simple cutoff using the truncated potential at r_c = 2.4 σ. (the time at r_c = 2.4 σ for a 12 processor system is 0.097 s per cycles (one cycle corresponds to N translations). The JAN method is 11% faster than the GL12 method. The use of the JAN method with the density updated every five MC cycles does not add significantly to the time of the simulation (note, this particular choice of frequency of update does not alter the results for the densities and the surface tension).

A good estimate of γ is obtained using a cutoff of r_c = 3 σ when the long-range corrections are applied during the course of the simulation run. For the coexisting densities, a cutoff of 4σ is required to obtain a converged estimate, even when the corrections are applied at every step. (The simulations at r_c = 4 σ are 1.8 times slower than the corresponding simulations at r_c = 3 σ.)

To avoid the use of the long-range corrections during the course of the simulation, a cutoff $r_c \geq$ 5.5 σ is required for the accurate calculation of the coexisting densities (these simulations will be 2.5 times slower than for a cutoff of 3 σ when using the GL12 and JAN methods). This value of r_c = 5.5 σ will provide a well-converged estimate for the surface tension, and the long-range correction to γ can be added at the end of the simulation using the correct densities in the method of Blokhuis (which is identical to the GL1 and JAN corrections for this cutoff).

6. CONCLUSIONS

The molecular modeling of two-phase fluid systems in slab geometries has been an area of active research over the past decades. A number of factors such as the system-sizes dependence and the appropriate routes to the surface tension and pressure have been resolved. Other issues such as the capillary waves and their effect on the surface tension[61] as well as the instability of the two-phase system close to the critical point[62] have been addressed using other approaches. There has been considerable work on the importance of the long-range corrections for this type of simulation, particularly on how to calculate them accurately and how to include them in a computationally efficient manner. In this work, we have pulled

DOI: 10.1021/acs.jctc.5b00377
J. Chem. Theory Comput. 2015, 11, 4573−4585

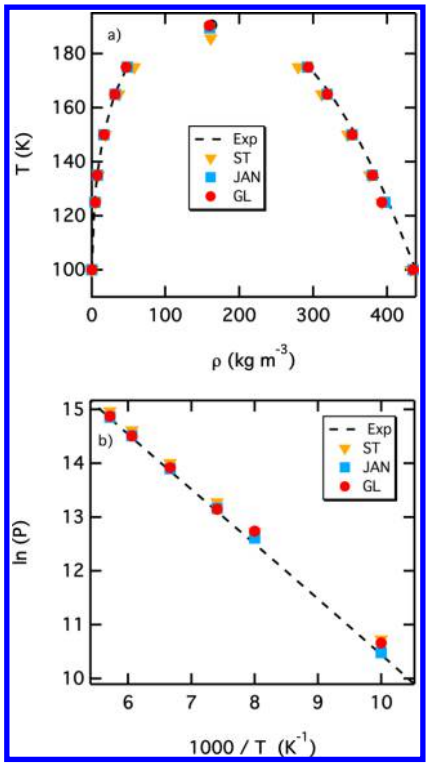

Figure 8. (a) Coexistence densities and (b) logarithmic vapor pressure versus inverse temperature calculated using the U_{ST}, U_{ST}^{GL}, and U_{ST}^{JAN} potential models.

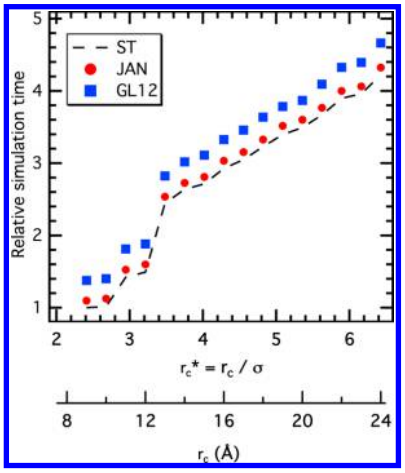

Figure 9. Relative simulation time of the simulations using a number of different cutoffs and the GL12 and JAN methods for applying the long-range corrections. The timings presented are relative to a simple cutoff using the truncated potential at $r_c = 2.4\ \sigma$.

together a number of different approaches and compared them carefully so that we are now in a position to make some recommendations on the best approach.

The two most widely used methods that consider the long-range corrections to the configurational energy during the course of the simulation are those of Guo and Lu and that of Janeček. These two slab-based tail corrections methods are designed to provide profiles of the long-range corrections along the direction normal to the interface for the energy, pressure, and surface tension. They were thought to be expensive because they needed to be employed at every step of the calculation and they directly affect the phase space trajectory of the simulation.

We have shown that the two-term correction of Guo and Lu (GL12) and the method of Janeček (JAN) give almost identical results for the interfacial properties when applied to the same set of configurations. The simpler GL1 method produces the same coexisting densities as GL12 and JAN but produces values of surface tension which are 5% higher than those of GL12 and JAN for $r_c < 5\ \sigma$. We would not recommend using GL1 for the calculation of γ. The GL12 method requires the calculation of a double integral of the density differences and adds ca. 11% to the time of a calculation compared to the truncated potential. Since the JAN method produces the same results as GL12, adds almost no time to the calculation, and is simpler to program, we recommend its use for temperatures away from the critical point when a stable slab exists. These conclusions on timings apply to the case in which the energy correction is applied at every step but when the underlying density profile is updated only every 10 cycles. With use of the JAN method for the calculation of γ, we recommend a cutoff of $r_c \geq 3\ \sigma$. The important and significant long-range correction to the pressure tensor and the surface tension can also be applied at each step using the JAN method (see eqs 28−32). It can also be applied accurately at the end of the calculation using the Blokhuis method (eq 24) as long as the coexisting densities are known accurately.

The convergence of the coexisting densities with the cutoff is slower than for the surface tension. We would recommend using a cutoff of at least 4.5 σ to obtain accurate values of these densities even with the long-range correction included at each step. The surface tension can be calculated without using the long-range correction at each step. In this approach we would recommend the use of the Blokhuis method with $r_c \geq 4\ \sigma$. For the calculation of the coexisting densities, we would recommend a value of $r_c \geq 5.5\ \sigma$.

We have made these conclusions for a model of Lennard-Jones fluid at two different temperatures. GL12 and JAN methods are equivalent up to 0.9 T_C. What happens for more complicated molecular fluid? Even in the case where the electrostatic interactions play a major role, the long-range correction to the dispersion interaction remains important[25,49] and it is necessary to add a correction for each term in the site−site potential. The conclusions will also be valid for fluid mixtures. However, in this case the density profile of a particular component may not be well represented by a tanh function, *e.g.*, where one component is adsorbed at the gas−liquid interface of the other component as is the case for CO_2/H_2O. In this case, we would recommend avoiding the Blokhuis correction and using the JAN correction during the course of the run. We note that the method of Janeček can be readily extended to more complicated functional forms than the Lennard-Jones potential. For more accurate two-body potentials (for example, the Barker Fisher Watts potential[44,60]),), the decay at large r is faster than r^{-6} and the conclusions that we make for the Lennard-Jones potential are equally valid.

We have also shown that the use of a truncated and shifted potential for the surface tension does not produce a converged result for any of the cutoffs discussed in this work and should be avoided. To simulate the surface tension close to the critical point ($T > 0.9\ T_C$), we need to use a finite-size scaling method.[62]

Our overall conclusion, is that an efficient accurate method for adding the long-range correction in these slab simulations is

DOI: 10.1021/acs.jctc.5b00377
J. Chem. Theory Comput. 2015, 11, 4573−4585

to use the Janeček method to estimate the long-range correction at each step of the simulation. The long-range correction to γ should also be calculated at each step using the Janeček method and added to the intrinsic calculation of γ. A cutoff between $r_c = 3.0\ \sigma$ and $r_c = 4.0\ \sigma$ can be then employed.

AUTHOR INFORMATION

Corresponding Author

*E-mail: Patrice.Malfreyt@univ-bpclermont.fr.

Notes

The authors declare no competing financial interest.

REFERENCES

(1) Liu, K. S. Phase Separation of Lennard-Jones Systems: A Film in Equilibrium with Vapor. *J. Chem. Phys.* **1974**, *60*, 4226−4230.

(2) Lee, J. K.; Barker, J. A.; Pound, G. M. Surface Structure and Surface Tension: Perturbation Theory and Monte Carlo Calculation. *J. Chem. Phys.* **1974**, *60*, 1976−1980.

(3) Chapela, G. A.; Saville, G.; Rowlinson, J. S. Computer Simulation of the Gas/Liquid Surface. *Faraday Discuss. Chem. Soc.* **1975**, *59*, 22−28.

(4) Rao, M.; Levesque, D. Surface Structure of a Liquid Film. *J. Chem. Phys.* **1976**, *65*, 3233−3236.

(5) Chapela, G. A.; Saville, G.; Thompson, S. M.; Rowlinson, J. S. Computer Simulation of a Gas-Liquid Surface. Part 1. *J. Chem. Soc., Faraday Trans. 2* **1977**, *73*, 1133−1144.

(6) Orea, P.; Lopez-Lemus, J.; Alejandre, J. Oscillatory Surface Tension due to Finite-Size effects. *J. Chem. Phys.* **2005**, *123*, 114702.

(7) Gonzalez-Melchor, M.; Orea, P.; Lopez-Lemus, J.; Bresme, F.; Alejandre, J. Stress Anisotropy Induced by Periodic Boundary Conditions. *J. Chem. Phys.* **2005**, *122*, 094503.

(8) Errington, J. R.; Kofke, D. A. Calculation of Surface Tension via Area Sampling. *J. Chem. Phys.* **2007**, *127*, 174709.

(9) Biscay, F.; Ghoufi, A.; Goujon, F.; Lachet, V.; Malfreyt, P. Calculation of the Surface Tension from Monte Carlo Simulations: Does the Model Impact on the Finite-Size Effects? *J. Chem. Phys.* **2009**, *130*, 184710.

(10) Werth, S.; Lishchuk, S. V.; Horsch, M.; Hasse, H. The Inflence of the Liquid Slab Thickness on the Planar Vapor-Liquid Interfacial Tension. *Phys. A* **2013**, *392*, 2359−2367.

(11) Trokhymchuk, A.; Alejandre, J. Computer Simulations of Liquid/Vapor Interface in Lennard-Jones Fluids: Some Questions and Answers. *J. Chem. Phys.* **1999**, *111*, 8510−8523.

(12) Lopez-Lemus, J.; Alejandre, J. Thermodynamic and Transport Properties of Simple Fluids using Lattice Sums: Bulk Phases and Liquid-Vapour Interface. *Mol. Phys.* **2002**, *100*, 2983−2992.

(13) Grosfils, P.; Lutsko, J. F. Dependence of the Liquid-Vapor Surface Tension on the Range of Interaction: A Test of the Law of Corresponding States. *J. Chem. Phys.* **2009**, *130*, 054703.

(14) Ibergay, C.; Ghoufi, A.; Goujon, F.; Ungerer, P.; Boutin, A.; Rousseau, B.; Malfreyt, P. Molecular Simulations of the *n*-Alkane Liquid-Vapor Interface: Interfacial Properties and Their Long Range Corrections. *Phys. Rev. E: Stat., Nonlinear, Soft Matter Phys.* **2007**, *75*, 051602.

(15) Gloor, G. J.; Jackson, G.; Blas, F. J.; de Miguel, E. Test-Area Simulation Method for the Direct Determination of the Interfacial Tension of Systems with Continuous or Discontinuous Potentials. *J. Chem. Phys.* **2005**, *123*, 134703.

(16) Salomons, E.; Mareschal, M. Surface Tension, Adsorption and Surface Entropy of Liquid-Vapour Systems by Atomistic Simulation. *J. Phys.: Condens. Matter* **1991**, *3*, 3645−3661.

(17) Salomons, E.; Mareschal, M. Atomistic Simulation of Liquid-Vapour Coexistence:Binary Mixtures. *J. Phys.: Condens. Matter* **1991**, *3*, 9215−9228.

(18) Blokhuis, E. M.; Bedeaux, D.; Holcomb, C. D.; Zollweg, J. A. Tail Corrections to the Surface Tension of a Lennard-Jones Liquid-Vapour Interface. *Mol. Phys.* **1995**, *85*, 665−669.

(19) Guo, M.; Lu, B. C. Y. Long Range Corrections to Thermodynamic Properties of Inhomogeneous Systems with Planar Interfaces. *J. Chem. Phys.* **1997**, *106*, 3688−3695.

(20) Goujon, F.; Malfreyt, P.; Boutin, A.; Fuchs, A. H. Direct Monte Carlo Simulations of the Equilibrium Properties of n-Pentane Liquid-Vapor Interface. *J. Chem. Phys.* **2002**, *116*, 8106−8117.

(21) Goujon, F.; Malfreyt, P.; Simon, J. M.; Boutin, A.; Rousseau, B.; Fuchs, A. H. Monte Carlo Versus Molecular Dynamics Simulations in Heterogeneous Systems: An Application to the n-Pentane Liquid-Vapor Interface. *J. Chem. Phys.* **2004**, *121*, 12559−12571.

(22) Janeček, J. Long Range Corrections in Inhomogeneous Simulations. *J. Phys. Chem. B* **2006**, *110*, 6264−6269.

(23) Shen, V. K.; Mountain, R. D.; Errington, J. R. Comparative Study of the Effect of Tail Corrections on Surface Tension Determined by Molecular Simulation. *J. Phys. Chem. B* **2007**, *111*, 6198−6207.

(24) Guo, M.; Peng, D.-Y.; Lu, B. C.-Y. On the Long-Range Corrections to Computer Simulation Results for the Lennard-Jones Vapor-Liquid Interface. *Fluid Phase Equilib.* **1997**, *130*, 19−30.

(25) Míguez, J. M.; Pineiro, M. M.; Blas, F. J. Influence of the Long-Range Corrections on the Interfacial Properties of Molecular Models using Monte Carlo Simulation. *J. Chem. Phys.* **2013**, *138*, 034707.

(26) Allen, M. P.; Tildesley, D. J. *Computer Simulations of Liquids*; Clarendon Press: Oxford, U.K., 1987.

(27) Lopez-Lemus, J.; Alejandre, J. Simulation of Phase Equilibria and Interfacial Properties of Binary Mixtures on the Liquid-Vapour Interface using Lattice Sums. *Mol. Phys.* **2003**, *101*, 743−751.

(28) Fowler, R. H. A Tentative Statistical Theory of Macleod's Equation for Surface Tension, and the Parachor. *Proc. R. Soc. London, Ser. A* **1937**, *159*, 229−246.

(29) Freeman, K. S. C.; McDonald, I. R. Molecular Theory of Surface Tension. *Mol. Phys.* **1973**, *26*, 529−537.

(30) Kirkwood, J. G.; Buff, F. P. The Statistical Mechanical Theory of Surface Tension. *J. Chem. Phys.* **1949**, *17*, 338−343.

(31) Alejandre, J.; Tildesley, D. J.; Chapela, G. A. Molecular Dynamics Simulation of the Orthobaric Densities and Surface Tension of Water. *J. Chem. Phys.* **1995**, *102*, 4574−4573.

(32) Vega, C.; de Miguel, E. Surface Tension of the Most Popular Models of Water by using the Test-Area Simulation Method. *J. Chem. Phys.* **2007**, *126*, 154707.

(33) Alejandre, J.; Tildesley, D. J.; Chapela, G. A. Fluid Phase Equilibria Using Molecular Dynamics: the Surface Tension of Chlorine and Hexane. *Mol. Phys.* **1995**, *85*, 651−663.

(34) Biscay, F.; Ghoufi, A.; Goujon, F.; Lachet, V.; Malfreyt, P. Surface Tensions of Linear and Branched Alkanes from Monte Carlo Simulations using the Anisotropic United Atom Model. *J. Phys. Chem. B* **2008**, *112*, 13885−13897.

(35) Guo, M.; Lu, B. C. Y. Long Range Corrections to Mixture Properties of Inhomogeneous Systems. *J. Chem. Phys.* **1998**, *109*, 1134.

(36) Mecke, M.; Winkelmann, J.; Fischer, J. Molecular Dynamics Simulation of the Liquid-Vapor Interface: The Lennard-Jones Fluid. *J. Chem. Phys.* **1997**, *107*, 9264−9270.

(37) Mecke, M.; Winkelmann, J.; Fischer, J. Molecular Dynamics Simulation of the Liquid-Vapor Interface: Binary Mixtures of Lennard-Jones Fluids. *J. Chem. Phys.* **1999**, *110*, 1188−1194.

(38) MacDowell, L. G.; Blas, F. J. Surface Tension of Fully Flexible Lennard-Jones Chains: Role of Long-Range Corrections. *J. Chem. Phys.* **2009**, *131*, 074705.

(39) Martinez-Ruiz, F. J.; Blas, F. J.; Mendiboure, B.; Bravo, A. I. M.-V. Effect of Dispersive Long-Range Corrections to the Pressure Tensor. The Vapour-Liquid Interfacial Properties of the Lennard-Jones System Revisited. *J. Chem. Phys.* **2014**, *141*, 184701.

(40) Biscay, F.; Ghoufi, A.; Lachet, V.; Malfreyt, P. Prediction of the Surface Tension of the Liquid-Vapor Interface of Alcohols from Monte Carlo Simulations. *J. Phys. Chem. C* **2011**, *115*, 8670−8683.

(41) Neyt, J. C.; Wender, A.; Lachet, V.; Ghoufi, A.; Malfreyt, P. Molecular Modeling of the Liquid-Vapor Interfaces of a Multi-Component Mixture: Prediction of the Coexisting Densities and

DOI: 10.1021/acs.jctc.5b00377
J. Chem. Theory Comput. 2015, 11, 4573−4585

Surface Tensions at Different Pressures and Gas Compositions. *J. Chem. Phys.* **2013**, *139*, 024701.
(42) Janeček, J.; Krienke, H.; Schmeer, G. Interfacial Properties of Cyclic Hydrocarbons: A Monte Carlo Study. *J. Phys. Chem. B* **2006**, *110*, 6916−6923.
(43) Benet, J.; MacDowell, L. G.; Menduiña, C. Liquid-Vapor Phase Equilibria and Surface Tension of Ethane As Predicted by the TraPPE and OPLS Models. *J. Chem. Eng. Data* **2010**, *55*, 5465−5470.
(44) Goujon, F.; Malfreyt, P.; Tildesley, D. J. The Gas-Liquid Surface Tension of Argon: A Reconciliation between Experiment and Simulation. *J. Chem. Phys.* **2014**, *140*, 244710.
(45) Irving, J. H.; Kirkwood, J. G. The Statistical Mechanical Theory of Transport Processes. IV. The Equations of Hydrodynamics. *J. Chem. Phys.* **1950**, *18*, 817−829.
(46) Rowlinson, J. S.; Widom, B. *Molecular Theory of Capillarity*; Clarendon Press: Oxford, U.K., 1982.
(47) in 't Veld, P. J.; Ismail, A. E.; Grest, G. S. Application of Ewald Summations to Long-Range Dispersion Forces. *J. Chem. Phys.* **2007**, *127*, 144711.
(48) Alejandre, J.; Chapela, G. A. The surface Tension of TIP4P/2005 Water Model using the Ewald Sums for the Dispersion Interactions. *J. Chem. Phys.* **2010**, *132*, 014701.
(49) Isele-Holder, R. E.; Mitchell, W.; Ismail, A. E. Development and Application of a Particle-Particle Particle-Mesh Ewald Method for Dispersion Interactions. *J. Chem. Phys.* **2012**, *137*, 174107.
(50) Isele-Holder, R. E.; Mitchell, W.; Hammond, J. R.; Kohlmeyer, A.; Ismail, A. E. Reconsidering Dispersion Potentials: Reduced Cutoffs in Mesh-Based Ewald Solvers Can Be Faster Than Truncation. *J. Chem. Theory Comput.* **2013**, *9*, 5412−5420.
(51) Tameling, D.; Springer, P.; Bientinesi, P.; Ismail, A. E. Multilevel Summation for Dispersion: A Linear-Time Algorithm for r^{-6} Potentials. *J. Chem. Phys.* **2014**, *140*, 024105.
(52) Möller, D.; Oprzynski, J.; Müller, A.; Fischer, J. Prediction of Thermodynamic Properties of Fluid Mixtures by Molecular Dynamics Simulations: Methane-Ethane. *Mol. Phys.* **1992**, *75*, 363−378.
(53) Walton, J. P. R. B.; Tildesley, D. J.; Rowlinson, J. S.; Henderson, J. R. The pressure Tensor at the Planar Surface of a Liquid. *Mol. Phys.* **1983**, *48*, 1357−1368.
(54) Walton, J. P. R. B.; Gubbins, K. E. The Pressure Tensor in an Inhomogeneous Fluid of Non-spherical Molecules. *Mol. Phys.* **1985**, *55*, 679−688.
(55) Janeček, J.; Krienke, H.; Schmeer, G. Inhomogeneous Monte Carlo Simulation of the Vapor-Liquid Equilibrium of Benzene Between 300 and 530 K. *Condens. Matter Phys.* **2007**, *10*, 415−423.
(56) Janeček, J. Effect of the Interfacial Area on the Equilibrium Properties of Lennard-Jones Fluid. *J. Chem. Phys.* **2009**, *131*, 124513.
(57) Chen, L.-J. Area Dependence of the Surface Tension of a Lennard-Jones Fluid from Molecular Dynamics Simulations. *J. Chem. Phys.* **1995**, *103*, 10214.
(58) Lemmon, E. W.; McLinden, M. O.; Friend, D. G. Thermophysical Properties of Fluid Systems, in *NIST Chemistry Webbook*, NIST Standard Reference Database No. 69; Linstrom, P. J., Mallard, W. G., Eds.; National Institute of Standards and Technology: Gaithersburg, MD, USA, 2005; http://webbook.nist.gov (accessed on Mar. 13, 2015) .
(59) Werth, S.; Horsch, M.; Vrabec, J.; Hasse, H. Comment on "The Gas-Liquid Surface Tension of Argon: A Reconciliation between Experiment and Simulation" [J. Chem. Phys. 140, 244710 (2014)]. *J. Chem. Phys.* **2015**, *142*, 107101.
(60) Goujon, F.; Malfreyt, P.; Tildesley, D. J. Response to "Comment on 'The Gas-Liquid Surface Tension of Argon: A Reconciliation between Experiment and Simulation" [J. Chem. Phys. 142, 107101 (2015)]. *J. Chem. Phys.* **2015**, *142*, 107102.
(61) Chacón, E.; Tarazona, P. Intrinsic Profiles Beyond the Capillary Wave Theory: A Monte Carlo study. *Phys. Rev. Lett.* **2003**, *91*, 166103.
(62) Potoff, J. J.; Panagiotopoulos, A. Surface Tension of the Three-Dimensional Lennard-Jones Fluid from Histogram Reweighting Monte Carlo Simulations. *J. Chem. Phys.* **2000**, *112*, 6411−6415.

DOI: 10.1021/acs.jctc.5b00377
J. Chem. Theory Comput. 2015, 11, 4573−4585